

A first-principles study of carbon-related energy levels in GaN: Part I - Complexes formed by substitutional/interstitial carbons and gallium/nitrogen vacancies

Masahiko Matsubara and Enrico Bellotti

*Department of Electrical and Computer Engineering,
Boston University, 8 St. Mary's Street, Boston, MA 02215, USA*

(Dated: June 20, 2017)

Various forms of carbon based complexes in GaN are studied with first-principles calculations employing Heyd-Scuseria-Ernzerhof hybrid functional within the framework of density functional theory. We consider carbon complexes made of the combinations of single impurities, i.e. $C_N - C_{Ga}$, $C_I - C_N$ and $C_I - C_{Ga}$, where C_N , C_{Ga} and C_I denote C substituting nitrogen, C substituting gallium and interstitial C, respectively, and of neighboring gallium/nitrogen vacancies (V_{Ga}/V_N), i.e. $C_N - V_{Ga}$ and $C_{Ga} - V_N$. Formation energies are computed for all these configurations with different charge states after full geometry optimizations. From our calculated formation energies, thermodynamic transition levels are evaluated, which are related to the thermal activation energies observed in experimental techniques such as deep level transient spectroscopy. Furthermore, the lattice relaxation energies (Franck-Condon shift) are computed to obtain optical activation energies, which are observed in experimental techniques such as deep level optical spectroscopy. We compare our calculated values of activation energies with the energies of experimentally observed C-related trap levels and identify the physical origins of these traps, which were unknown before.

PACS numbers: 61.72.J-, 61.72.uj, 71.15.Mb, 71.55.Eq

I. INTRODUCTION

Carbon inclusion is unavoidable when growing GaN layers by metal organic chemical vapor deposition (MOCVD) technique due to several reasons: metalorganic species used as source materials, contaminants in the source gases and hydrocarbons from graphite susceptors. As a result, un-intentional carbon doping is present in GaN layers as impurities and can assume different configurations in the crystal lattice. The amount of incorporated carbon depends on the growth temperature¹ and pressure². Even in the case of growth performed with molecular beam epitaxy (MBE), GaN samples are contaminated by carbon impurities as soon as they are removed from vacuum and various mitigation approaches are being developed.³⁻⁵

On the other hand, intentional carbon doping is routinely used to obtain semi-insulating layers of GaN (GaN:C) that are critical for the fabrication of high electron mobility transistors (HEMTs)^{6,7}. At the same time, the presence of a significant amount of carbon in the substrate, may lead to deep level traps acting as recombination centers in the band gap, which are detrimental to the HEMTs performance, potentially leading to current collapse and kink effect^{8,9}. Therefore in order to understand the effect of carbon on the devices' operation and improve their performance it is important to identify the physical origins of C-related deep level traps.

Earlier theoretical calculations based on density functional theory (DFT) within local density approximation (LDA)¹⁰⁻¹⁴ suggested that C could exist as substitutional forms in GaN, specifically C substituting N (C_N) and C substituting Ga (C_{Ga}). It was also shown that C_N acts as a shallow¹⁵ acceptor with ~ 0.3 eV activation energy and C_{Ga} acts as a shallow donor with activation energy with

~ 0.2 eV. It was also suggested that self-compensation by C_{Ga} and C_N pins the Fermi level in the middle of band gap and this explains the high resistivity of GaN:C layer¹⁶. Another possible form of a single interstitial impurity, C_I , was predicted to show amphoteric behavior, acting as a deep acceptor in *n*-type GaN and as a deep donor in *p*-type GaN¹⁴. Furthermore, the activation energy for this acceptor level due to C_I has predicted to be ~ 1.1 eV.

From the experimental standpoint, a significant number of studies to understand the trap levels, specifically the energy states in the band-gap, in carbon doped GaN have been performed using a variety of techniques. Among these, photoionization spectroscopy (PS)^{8,17}, deep level transient spectroscopy (DLTS), including minority carrier transient spectroscopy (MCTS) and photoinduced current transient spectroscopy (PICTS)¹⁸⁻²⁴, deep level optical spectroscopy (DLOS)^{18-20,25} and cathodoluminescence (CL) measurement^{16,24}. DLTS, MCTS and PICTS have been primarily employed to detect trap levels close to the band edges (within ~ 1.0 eV). Techniques based on optical methods such as DLOS are used mainly to detect deeper trap levels, in an energy range close to the center of the band gap. Combinations of different types of techniques makes it possible to cover entire band gap region and potentially detect all existing trap levels.

Using PS technique, Klein *et al.* showed that one of two kinds of deep traps (with absorption threshold at 2.85 eV), which is responsible for the current collapse of AlGaIn/GaN HEMT, has a carbon origin because its concentration tracks the carbon doping level¹⁷. Hierro *et al.* using DLOS measurement which is able to determine that a trap level located 1.35 eV below the conduction band minimum (CBM, E_c) was related to carbon¹⁸.

Armstrong *et al.* investigated the origin of a number of deep level traps in GaN using a combination of DLTS, DLOS and steady-state photocapacitance (SSPC) techniques^{19,20}. Two of the energy levels obtained by DLTS were ascribed to carbon. One was located 0.11 eV below the CBM, and its origin was assigned to C_{Ga} , based on previous LDA calculated results. The other trap level appeared at $E_v + 0.9$ eV, where E_v is the energy of the valence band maximum (VBM), but its physical origin was unknown. In addition, four more levels that were obtained by the combination of DLOS and SSPC were ascribed to carbon. Based on existing LDA result¹⁴, a trap energy level at $E_c - 1.35$ eV was assigned to an acceptor state of interstitial carbon (C_{I}). Two traps at $E_c - 1.94$ eV and $E_c - 3.0$ eV were C-related, but their physical forms remained unknown. A trap at $E_c - 3.28$ eV was assigned to an acceptor level of C_{N} , once again, based on LDA result¹⁴.

Shah and coworkers performed DLTS and MCTS measurements²³ and inferred that an energy level at $E_c - 0.13$ eV was possibly related to C_{Ga} and behaved as an electron trap state. Furthermore, two energy levels responsible for trapping holes were observed and were also related to C. One was at $E_c - 3.20$ eV with C_{N} assignment and the other at $E_c - 2.69$ eV with C_{N} -related defects or gallium vacancy. Polyakov *et al.* studied deep levels by photocurrent spectra measurements and PICTS. With the former method three C-related trap levels with optical threshold near 1.3–1.4 eV, 2.7–2.8 eV and 3 eV were observed. The first was attributed to C_{I} acceptor state, whereas the other two were left unassigned. More recent experimental result, carried out by Honda *et al.* using MCTS measurements, indicated that a hole trapping state may be present at $E_v + 0.86$ eV and was assigned to C_{N} based on recent DFT calculation employing hybrid functionals²². They also concluded that one electron trap at $E_c - 0.40$ eV was associated with C, but did not specify its physical form.

From the theoretical standpoint, the majority of studies performed to understand the nature of carbon in GaN have been carried out using DFT within the LDA approximation.^{10,11,13,14} Only recently, a small number of investigations^{26–29} have employed more sophisticated DFT approaches based on hybrid functionals, with the intent to overcome the limitations of LDA, and obtain a more reliable energetics for the various carbon configurations in GaN. Among these recent studies, DFT calculations using Heyd-Scuseria-Ernzerhof (HSE) hybrid density functionals for single carbon impurities, C_{N} and C_{Ga} , were reported^{26–28}. Unlike in previous LDA results, these calculations indicates that C_{N} may not be a shallow but a deep acceptor with ~ 0.9 eV activation energy, which means that C cannot be used as a p -type donor in GaN. Furthermore, recent HSE-based calculations, indicates that the acceptor level of C_{I} is ~ 0.4 eV as opposed to the values of ~ 1.1 eV obtained using LDA.²⁸ These new outcomes, suggest that the assignments of experimentally observed trap levels based on earlier LDA results

should be re-examined using more reliable approaches, such as HSE hybrid density functionals, that could provide a more accurate picture of the system energetics.

The aim of this work is twofold, first, we intend to perform a comprehensive study of the formation energies of single carbon impurity and complexes in GaN using state-of-the-art DFT and HSE hybrid density functionals. Specifically we intend to focus on the role of complexes about which very little is known, although C_{N} is considered as the dominant form as a single carbon impurity especially in n -type GaN in Ga-rich conditions. Indeed, the origins of some of the experimentally observed C-related trap levels are assigned to C_{N} as described above. Second, we intend to perform a systematic comparison of the numerical results with the available experimental data with two specific goals in mind: establish which energy level can be reliably assigned to a given configuration, and for which energy level additional experimental and theoretical work is needed. We want to emphasize this last issue, since there are several experimentally observed C-related energy levels, whose physical forms are still unknown.

This manuscript focuses on the complexes that carbon forms with Ga, N and their vacancies. Furthermore, this work is a companion to a second manuscript³⁰ in which we present the investigation of complexes that carbon forms in GaN with silicon, oxygen and hydrogen and we discuss their relative concentrations.

This paper is organized as follows. In Section II, the details of the computational model are presented and the theoretical formulations of the formation energies and transition levels are provided. Furthermore we describe what kind of convergence studies have been performed to determine the supercell size to be used in the case of charged defects and complexes. In Section III, we will outline our calculated results that will be discussed in Section IV. Finally concluding remarks are given in Section V.

II. METHODS

In this section the computational approach is outlined. First the computational framework is presented. Subsequently the model used to evaluate the formation energy is given, and finally the effect of the supercell size on formation energy is discussed.

A. Computational Approach

The calculations presented in this work were carried out using the projector augmented wave (PAW) method³¹ implemented in the VASP code³². The main results were obtained using Heyd-Scuseria-Ernzerhof (HSE) hybrid functionals³³. Additionally, convergence tests were also performed using standard Perdew-Burke-Ernzerhof (PBE)³⁴ functionals. The semicore Ga $3d$ elec-

TABLE I. Calculated values for lattice constants, energy gap, formation enthalpy and static dielectric constant. Experimental results are also given.

	a (Å)	c (Å)	u	E_{gap} (eV)	ΔH_f (eV)	ϵ_0^a
Calc.	3.178	5.171	0.377	3.45	-1.18	9.48
Expt.	3.190 ^b	5.189 ^b	0.375 ^b	3.5 ^c	-1.63 ^d / -1.14^e	9.8 ^f

^a averaged value over $E_{\parallel c}$ and $E_{\perp c}$ components.

^b Ref. 36.

^c Ref. 35.

^d Ref. 37.

^e Ref. 38.

^f Ref. 39.

trons were included as valence, since treating Ga $3d$ electrons as core caused relatively large errors (~ 0.5 eV) in the formation energies for carbon complexes. Furthermore, in the case of HSE, in order to reproduce experimental band gap value (3.5 eV³⁵), the amount of exact exchange was taken to be 28% (giving 3.45 eV band gap value). Spin is explicitly considered (spin-unrestricted) in all the calculations. Finally, a 425 eV cutoff energy was used. During the structural optimization procedure to obtain the total energy of different configurations, the atomic positions were allowed to change until the largest force component was less than 0.05 eV/Å. The bulk parameters obtained from fully optimized unit cell are summarized in Table I. Using these optimized lattice constants, a supercell containing total 96 atoms with orthorhombic shape was constructed and employed to study the carbon inclusions. The Brillouin zone is sampled on a mesh composed of a $2 \times 2 \times 2$ k -point grid. Convergence tests in PBE showed that the differences in formation energies between $2 \times 2 \times 2$ mesh and denser $5 \times 5 \times 5$ mesh were less than 50 meV. The same tests were also done in HSE, where $2 \times 2 \times 2$ mesh and $3 \times 3 \times 3$ mesh were compared. The differences in formation energies were less than 0.1 eV. In Fig. 1, the formation energies (its definition will be provided in the next section) for V_{Ga} in Ga-rich condition are presented for different k -point mesh both in PBE and HSE to show the convergence. Convergence tests performed to evaluate the dependence of the calculated values on the supercell size will be discussed in Section II C.

B. Defect Formation Energies and Thermodynamic Transition Levels

The formation energy (E_f^q) as a function of the Fermi energy (E_F), for a given defect configuration D was calculated with the following formula :

$$E_f^q(D, E_F) = E_{\text{tot}}^q(D) - E_{\text{bulk}} - \sum_X n_X \mu_X + q(E_F + E_v) + \Delta E_{\text{corr}}^q, \quad (1)$$

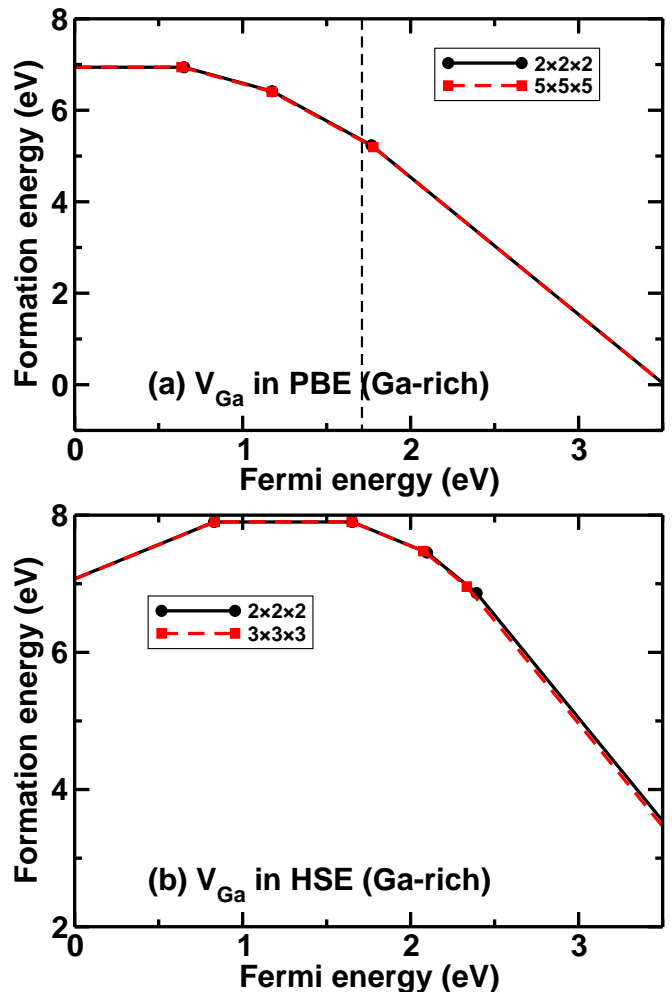


FIG. 1. Formation energies for Ga vacancy with different sets of k -point meshes in (a) PBE and (b) HSE. In the case of PBE, the $2 \times 2 \times 2$ and $5 \times 5 \times 5$ meshes are compared, whereas in the case of HSE $2 \times 2 \times 2$ and $3 \times 3 \times 3$ meshes are compared. Note that no band gap correction was done in the case of PBE (vertical dashed line at 1.71 eV denotes the calculated conduction band minimum).

where $E_{\text{tot}}^q(D)$ is the total energy of the system with a defect D in a charge state q , E_{bulk} the total energy of bulk wurtzite GaN, n_X the number of X (X = Ga, N or C) atoms removed from, or added to, the system with the chemical potential μ_X and E_v the energy of the valence band maximum (VBM). The last term is the correction for charged defects in the finite supercell. In this work, we have adopted the method proposed by Freysoldt *et al.* to calculate this correction term⁴⁰ using `sxdefectalign` program⁴¹.

The chemical potential for Ga (μ_{Ga}) was evaluated using bulk α -Ga and that for N (μ_{N}) determined using an isolated N_2 molecule. The value of μ_{C} was obtained from the calculated value for cubic diamond. Furthermore,

μ_{Ga} and μ_{N} satisfy the following condition

$$\mu_{\text{Ga}} + \mu_{\text{N}} = E(\text{Ga}) + \frac{1}{2}E(\text{N}_2) + \Delta H_f(\text{GaN}), \quad (2)$$

where $\Delta H_f(\text{GaN})$ is the formation enthalpy of GaN. In the Ga-rich limit, μ_{Ga} corresponds to the energy of bulk Ga ($E(\text{Ga})$), whereas in the N-rich limit, μ_{N} corresponds to the half value of the energy of N_2 ($\frac{1}{2}E(\text{N}_2)$). The thermodynamic transition energy is defined as the position of Fermi level at which the most stable charge state changes from q to q' :

$$\epsilon(q/q') = \frac{E_f^q(D, E_F = 0) - E_f^{q'}(D, E_F = 0)}{q' - q}. \quad (3)$$

Since this formulation of formation energy is based on thermodynamic equilibrium, the calculated transition level is directly related to the thermal activation energies obtained by thermal experimental technique such as DLTS. In addition, under thermodynamic equilibrium condition, the concentration, $[C]$, of an impurity with the formation energy E_f can be computed by the equation

$$[C] = N \exp\left(\frac{-E_f}{k_B T}\right), \quad (4)$$

where N is the number of defect sites per volume, k_B is the Boltzmann's constant and T is the growth temperature. As a result we expect that, the lower the formation energy is, the higher is the concentration of a specific defect configuration.

C. Supercell size for charged defects

Defect formation energies calculations are customarily performed within a periodic supercell approach. However, this approach, when applied to charged systems, is hampered by spurious Coulomb interactions between defect itself and its periodic images. In order to exclude this artificial effect, a number of correction schemes have been proposed^{40,42-45}. For this work we adopted the scheme proposed by Freysoldt *et al.*⁴⁰. We performed a series of test calculations for a number of significant defect configurations to check the convergence of the formation energies with respect to the supercell size (72-, 96-, 128-, 192-, 300-, 576-atom supercells). For these convergence test calculations, we used Perdew-Burke-Ernzerhof (PBE)³⁴ functionals, since convergence studies using HSE are more involved due to the computational demand of this approach. However, we can expect that if the convergence is reached in PBE, the same is true in HSE, because the correction scheme works better in hybrid functional calculations⁴⁶. Convergence test results (both corrected and uncorrected) are shown in Fig. 2 for C_I with 4+, 2+ and 1+ charge states and for $\text{C}_I - \text{C}_N$ with 3+ and 1+ charge states. In the case of C_I , convergence is already reached with a 72-atoms supercell both for corrected and uncorrected results with the 1+

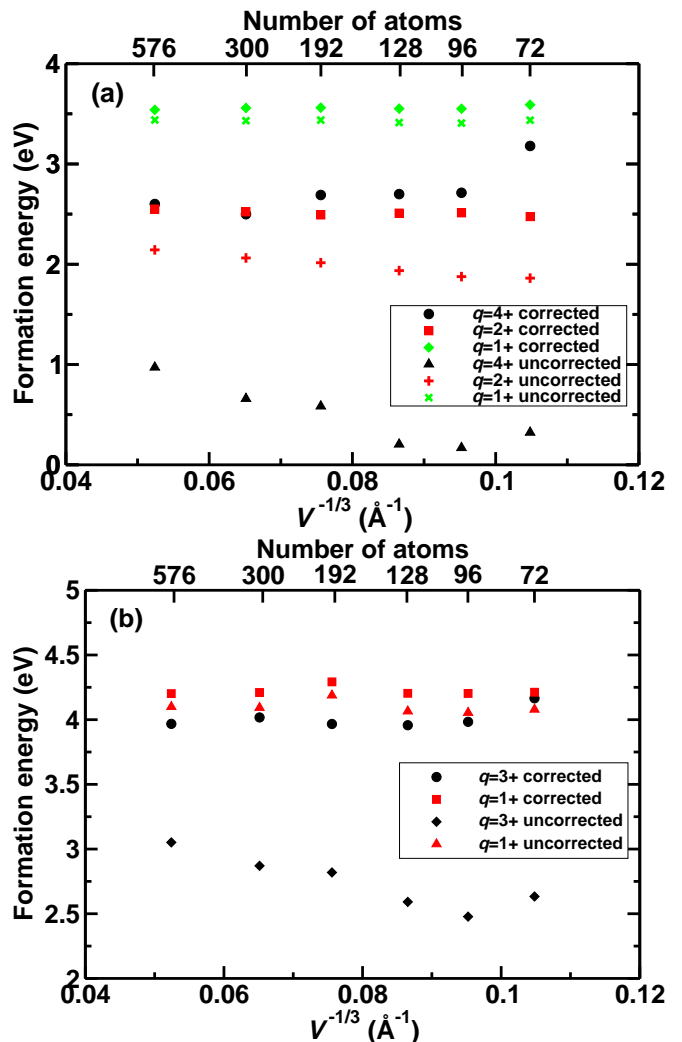


FIG. 2. Formation energies with respect to the supercell size for (a) C_I with 4+, 2+ and 1+ charge states and (b) $\text{C}_I - \text{C}_N$ complex with 3+, and 1+ charge states. Both corrected and uncorrected formation energies are plotted for comparison.

charge state. For the 2+ charge state, differences between corrected and uncorrected results are noticeable particularly in smaller size supercells. Nevertheless, the corrected formation energy is already well converged at the 72-atom supercell. Finally, for the 4+ charge state the differences between corrected and uncorrected results are sizable even at the 576-atom supercell. However, for this charge state, convergence is reached at the 96-atom supercell after the correction. In the case of complexes, such as $\text{C}_I - \text{C}_N$, the situation is almost the same as in the case of C_I . Specifically, for the 1+ charge state, the difference between corrected and uncorrected results are small and convergence is reached with the 72-atom supercell. For the 3+ charge state, differences between corrected and uncorrected results are large and the correction is significant. In this charge state, 96-atom supercell gives converged results after the correction is applied. Based on the outcome of these convergence studies, for our com-

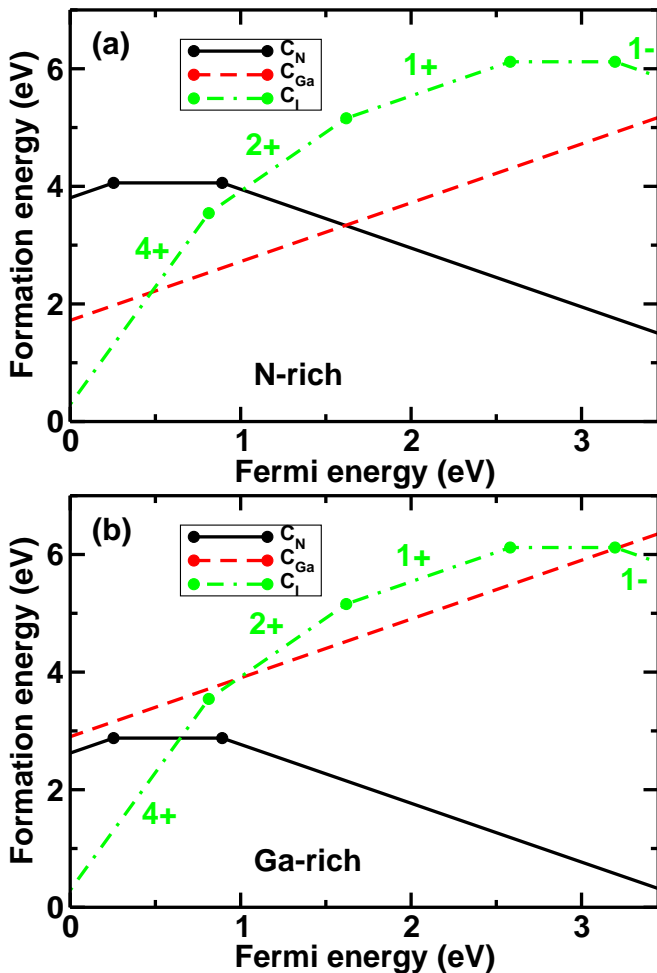


FIG. 3. Formation energies as a function of Fermi energy for C_N (solid line in black), C_{Ga} (dashed line in red) and C_I (dashed-dotted line in green) in (a) N-rich conditions and (b) Ga-rich conditions.

putation we adopted 96-atom supercell and between two and six integration points, to obtain accurate results with reasonable computational costs.

III. RESULTS

In this section we will briefly present the results obtained for single carbon impurities. Subsequently, we will discuss in details the outcome of the calculations for carbon complexes that have not been as extensively studied as the single carbon impurities.

A. Single carbon impurity

This section presents the results obtained using HSE for single carbon, substitutional and interstitial, impurities: C_{Ga} , C_N and C_I . The calculated formation energies for these defects are shown in Fig. 3, where only

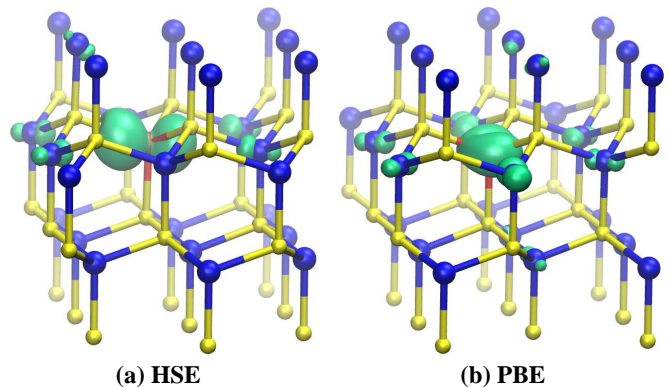


FIG. 4. Spin density of the C_N in the 0 (neutral) charge state obtained within (a) HSE and (b) PBE. Isosurface values are taken to be $0.05 \mu_B/\text{\AA}^3$.

the lowest energy states within the band gap are presented. Among them, our emphasis is on the C_I , because two substitutional cases, C_{Ga} and C_N , have been studied in detail both within LDA^{10–14} and HSE^{26–28}. For C_{Ga} and C_N we provide a summary of the structural and electronic properties in Table II together with the values from literature for comparison.

In the cases of C_N with $q = 0$ and $q = 1+$, their structures show large symmetry lowering due to the Jahn-Teller distortion, which are not seen in the standard LDA/GGA calculations⁴⁷. With the $q = 0$ case as an example, after the PBE relaxation, C_N occupies the high symmetric position, where the distance between N atom parallel to the c axis (1.96 Å) and those between N atoms perpendicular to the c axis (1.97 Å) are nearly the same. On the other hand, after the HSE relaxation, C–N distance perpendicular to the c axis (2.08 Å, average of three) becomes longer than the one parallel to the c axis (1.96 Å). The calculated spin densities are shown in Fig. 4. For the HSE result, the spin density shows clear directional preference along one of the C–Ga bonds, suggesting directional hole localization due to the asymmetric relaxation. On the other hand, for the PBE result, the spin density is more isotropic and directional localization is absent. We also checked the magnetic configuration with the hole localization direction along the c axis and found that this configuration has higher energy than the one shown in Fig. 4. In other structures, i.e. C_{Ga} and C_I as well as all the complex structures shown in the following subsection, such a clear (Jahn-Teller) distortion is not observed. Therefore this effect is specific for the C_N case.

In the case of C_I , there are plenty of possibilities for the position of C atom as an interstitial in GaN. In this work, we took the comprehensive study by Wright¹⁴ as our starting point. We considered an octahedral interstitial position (denoted as channel configuration in Ref. [14]), tetrahedral interstitial position, split interstitial position and bond center position as initial configurations of C and then a full structural optimization was performed

TABLE II. Comparison of the calculated structural and electronic properties of C_N and C_{Ga} in the different charge states q . The averaged bond change (Δl given in %) is defined as the change of C–N (C–Ga) bond lengths in C_{Ga} (C_N) against the bulk Ga–N bond values. Negative (positive) values describe the decrease (increase) of the bond lengths. The formation energies (E_f given in eV) in Ga-rich conditions are also presented.

Form	q	LDA ^a			LDA ^b			HSE ^c		HSE (this work)	
		Δl	E_f	Δl	E_f	Δl	E_f	Δl	E_f		
C_{Ga}	1+	-17.3	–	-19	$3.17 + E_F$	-26	$2.7 + E_F$	-19.5	$2.90 + E_F$		
	0	-18.1	5.7	–	6.45	–	–	–			
C_N	1+	–	–	–	–	+6.7	$2.6 + E_F$	+6.1	$2.62 + E_F$		
	0	-2.0	1.1	+0.3	2.62	+2.75	2.9	+2.2	2.88		
	1–	–	–	-1.2	$2.88 - E_F$	-2	$3.8 - E_F$	-1.0	$3.77 - E_F$		

^a Refs. 10 and 11.

^b Ref. 14.

^c Refs. 26 and 28.

for each geometry. After fully relaxing all the configurations we found that the tetrahedral position never becomes the most stable and the bond center position either takes higher formation energy in some charge states or relaxes into split interstitial positions in other charge states. Consequently, we focus on the octahedral and split interstitial positions. In the split interstitial configurations, a tilted C–N dimer replaces a N atom and, depending on the direction of the dimer, four different types were considered¹⁴. In type 1 and 4 split interstitial configurations, C takes higher and lower positions than N, respectively, and has two bonds with Ga atoms. In type 2 and 3, C takes lower and higher positions than N, respectively, and has one bond with a Ga atom. The structures of these five configurations (octahedral and four split interstitials) are shown in Fig. 5. The calculated formation energies for these C_I configurations are also reported in Fig. 3 together with substitutional cases.

We can notice first that, the octahedral interstitial configuration, shown in Fig. 5(a), is the most stable in the 4+ charge state⁴⁸, which, in turn, is more stable than substitutional cases, both in N-rich and Ga-rich conditions when the Fermi energy is located close to the VBM. In this configuration a C atom is surrounded by three N atoms, which are attracted by the positively charged C atom. When considering the 3+ charge state, the octahedral interstitial configuration is also more stable than the split interstitial configurations, but this charge state never becomes favorable within the band gap. In the case of other charge states, split interstitial configurations are favorable.

The four variants of split interstitial configurations have very similar formation energies in each charge state. In the 2+ charge state, type 3 split interstitial configuration, in Fig. 5(d), is the most favorable. In the 1+ charge state, type 1 split interstitial configuration [Fig. 5 (b)] is the most stable. In the case of 0 (neutral) charge state, type 2 split interstitial configuration is the most stable, but type 1 split interstitial configurations have almost identical formation energies within a 10 meV range. In the case of 1– charge state, type 2 split interstitial configuration is the most stable. Type 4 split interstitial

configuration becomes favorable in the 2– charge state, but this state is never stable within the band gap.

To conclude this section, Table III and Fig. 6 provide a summary of our results for C_I and we compare them with previously obtained LDA results¹⁴ and recently obtained HSE results²⁸. In Fig. 6, it can be seen that, in the case of LDA, the (0/2–) transition occurs at $E_c - 1.13$ eV, but in both HSE results the 2– charge state is never stable within band gap and the (0/–) transition level appears at $E_c - 0.25$ eV (our result), instead. Furthermore, the transition levels for (+/0) and (2+/+) obtained with HSE are shifted closer to CBM, whereas (4+/2+) level shows small shift closer to VBM. In the previous HSE result²⁸, 4+ charge state is not reported. Therefore the (4+/2+) transition level is absent. The positions of three other levels between our results and the results in Ref. 28 are different up to ~ 0.35 eV. The reason is not clear, but we may attribute it to the use of different pseudopotentials and cutoff energy. For the comparison of LDA and HSE results in Fig. 6, band edge alignment procedure^{49–51} was not performed due to the unavailability of the details of band gap correction procedure in Ref. 14. It is possible that there exists substantial amount of valence band off-set between LDA and HSE results.

B. Carbon complexes

For the carbon complexes we consider combinations of single impurity carbon, i.e. $C_N - C_{Ga}$, $C_I - C_N$ and $C_I - C_{Ga}$. Formation energies of these complexes as a function of Fermi level are shown in Fig. 7. Additionally, complexes of substitutional C with neighboring vacancies, i.e. $C_N - V_{Ga}$ and $C_{Ga} - V_N$ are also considered. Formation energies of these complexes are shown in Fig. 8.

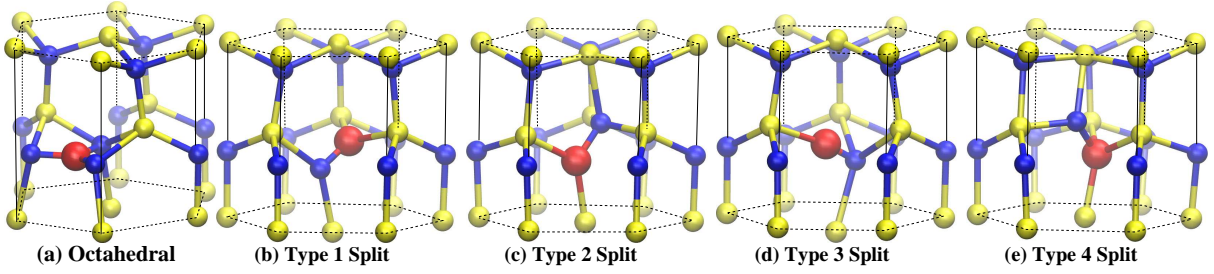


FIG. 5. Ball and stick representations of the positions of C_I in GaN. C atom is denoted by red sphere, while Ga and N are denoted by yellow and blue spheres, respectively. Relaxed configurations of (a) octahedral interstitial position with 4+ charge state, (b) type 1 split interstitial position with 1+ charge state, (c) type 2 split interstitial position with 1- charge state, (d) type 3 split interstitial position with 2+ charge state, (e) type 4 split interstitial positions with 2- charge state.

TABLE III. Comparison of the calculated structural and electronic properties of C_I in the different charge states q between the previous result in LDA¹⁴ and this work in HSE. The preferred forms with lowest energies in each charge state, the C-N bond lengths (l_{C-N} in Å) and the formation energies (E_f in eV) are presented.

q	form	LDA ^a		HSE (this work)		
		l_{C-N}	E_f	form	l_{C-N}	E_f
4+	octahedral	1.40	$1.76 + 4E_F$	octahedral	1.37	$0.29 + 4E_F$
3+	octahedral	–	$3.60 + 3E_F$	octahedral	1.45	$2.16 + 3E_F$
2+	split 1	–	$3.49 + 2E_F$	split 3	1.16	$1.92 + 2E_F$
1+	split 1	–	$4.67 + E_F$	split 1	1.23	$3.54 + E_F$
0	split 1	1.33	6.55	split 2	1.31	6.12
1-	split 3	–	$8.92 - E_F$	split 2	1.39	$9.31 - E_F$
2-	split 3	–	$11.26 - 2E_F$	split 4	1.47	$13.69 - 2E_F$

^a Ref. 14.

1. Binding energy

For these carbon complexes we calculate binding energies in addition to formation energies. The binding energy (E_B) for the complex denoted by $A - B$ is defined as

$$E_B^{q_A+q_B-q_{A-B}}(A-B, E_F) = E_f^{q_A}(A, E_F) + E_f^{q_B}(B, E_F) - E_f^{q_{A-B}}(A-B, E_F), \quad (5)$$

where the formation energies are chosen as the lowest energy configuration of each defect state at a particular Fermi energy. With this definition, the complex is stable (unstable), when E_B takes positive (negative) value. The calculated binding energy for $C_N - C_{Ga}$, $C_I - C_N$, $C_I - C_{Ga}$, $C_N - V_{Ga}$ and $C_{Ga} - V_N$ are shown in Fig. 9.

2. $C_N - C_{Ga}$

For this kind of complex two different configurations are possible and their relaxed structures are shown in Fig. 10. In one configuration, two C atoms are located along the c -axis and we will refer to it as the parallel configuration, as shown in Fig. 10(a). In the other configuration, two C atoms are located nearly perpendicular to the c -axis and this is referred to as the perpendicular

configuration shown in Fig. 10(b). Formation energies are calculated for both configurations and we find that the difference between them is very small, less than 0.1 eV, although the perpendicular configuration has lower formation energies than the parallel configuration. The formation energy of the perpendicular configuration $C_N - C_{Ga}$ complex is plotted in Fig. 7 with blue solid lines. Three charge states are favorable within the band gap. Up to 0.05 eV, the 2+ charge state is the most stable. Then for values of the Fermi energy up to 0.52 eV the 1+ charge state is the most stable. The neutral charge state instead, is the most stable when the Fermi energy is above 0.52 eV. Unlike previous LDA result¹⁴, negatively charged states are not present in the band gap. The C-C bond lengths and formation energies in each charge state are summarized in Table IV together with previous LDA results¹⁴ for comparison. Moreover, with a binding energy in excess of 1 eV (see Fig. 9), C_N and C_{Ga} form stable complexes in GaN. In the upper half of the fundamental band gap, the neutral charge state of this complex is the most favorable among all the C-complexes considered here, both in N-rich and Ga-rich limits. It should be noted that both C_{Ga} and C_N are positively charged near the VBM and are expected to repel each other. This may hinder the formation of the 2+ charge state of $C_N - C_{Ga}$ complex.

TABLE IV. Comparison of the calculated structural and electronic properties of $C_N - C_{Ga}$ in the different charge states q between the previous result in LDA¹⁴ and this work in HSE. The preferred forms, parallel (\parallel) or perpendicular (\perp) configurations, with lowest energies in each charge state, the C-C bond lengths (l_{C-C} in Å) and the formation energies (E_f in eV) are presented.

q	form	LDA ^a		HSE (this work)		
		l_{C-C}	E_f	form	l_{C-C}	E_f
2+	—	—	—	\perp	1.53	$4.49 + 2E_F$
1+	\parallel	—	$4.74 + E_F$	\perp	1.55	$4.54 + E_F$
0	\perp	1.5	4.81	\perp	1.56	5.05
1-	\perp	—	$8.19 - E_F$	\perp	1.57	$9.25 - E_F$

^a Ref. 14.

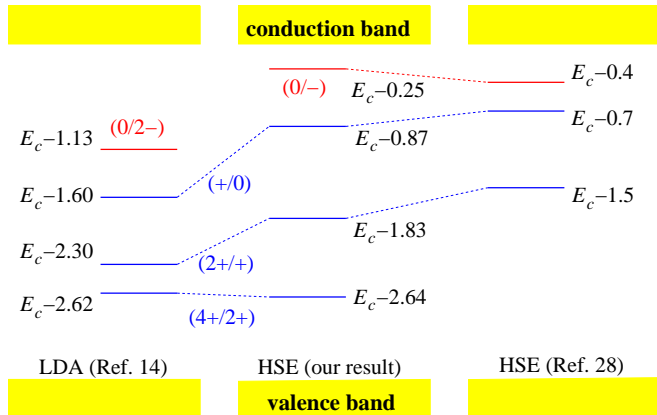


FIG. 6. Thermodynamic transition levels for C_I obtained by LDA¹⁴ (in left) and by HSE (our results in center and from Ref. 28 in right). The positions of the levels are measured from the conduction band minimum (E_c). Four transition levels appear in LDA and our HSE results, whereas the (4+/2+) transition level is absent in the results from Ref. 28. Three of four levels in LDA and our HSE results correspond to the same transitions, (4+/2+), (2+/+) and (+/0). The level closest to the E_c is (0/2-) in LDA result, whereas it is (0/-) in both HSE results. Note that no band edge alignment is considered.

3. $C_I - C_N$

Three different configurations are considered for the $C_I - C_N$ complex and they are shown in Fig. 11. The first configuration is the combination of octahedral configuration from C_I and C_N as shown in Fig. 11(a). The second configuration is composed of a Type 1 (Type 2) split interstitial C_I and C_N , where the high-positioned C atom has two bonds with Ga atoms. This is shown in Fig. 11(b). Finally, the third one is a combination of Type 3 (and Type 4) split interstitial C_I and C_N , where the high-positioned C atom has one bond with a Ga atom, as indicated in Fig. 11(c).

The formation energy values obtained for the $C_I - C_N$ complex are plotted (magenta dashed lines) in Fig. 7. The 3+, 1+ and neutral (0) charge are characterized by states positioned in the band gap. The 3+ charge state

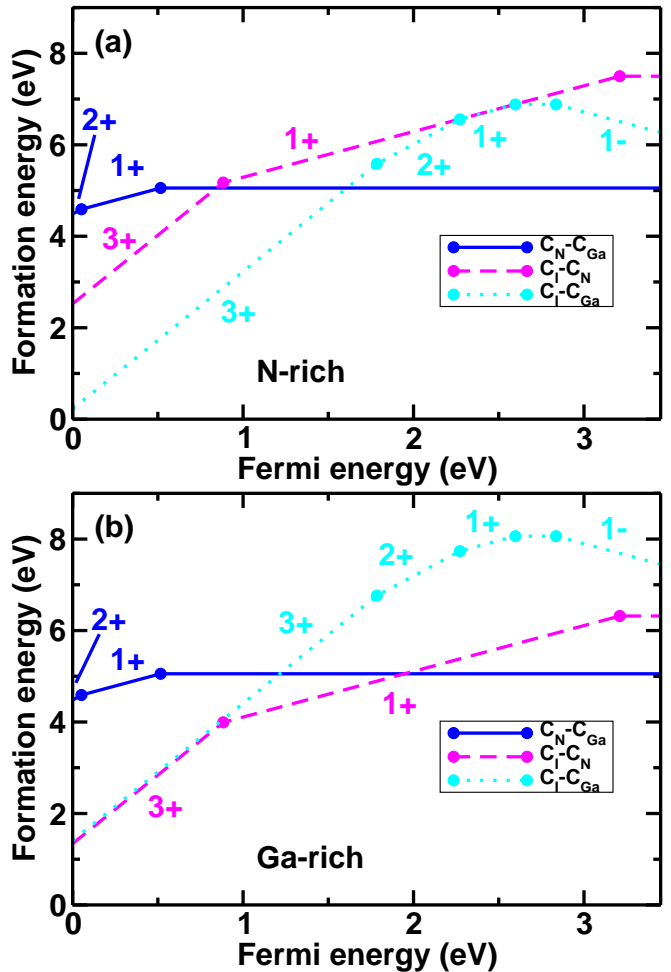


FIG. 7. Formation energies as a function of Fermi energy for $C_N - C_{Ga}$ (blue solid line), $C_I - C_N$ (magenta dashed line) and $C_I - C_{Ga}$ (cyan dotted line) in (a) N-rich conditions and (b) Ga-rich conditions.

is favorable for Fermi energies up to 0.88 eV, whereas the 1+ charge state is stable between 0.88 eV and 3.21 eV. Consequently, this complex, in 1+ state, mostly acts as a deep donor.

Additionally, in the Ga-rich limit, the 1+ charge state becomes the most favorable form among all the C-

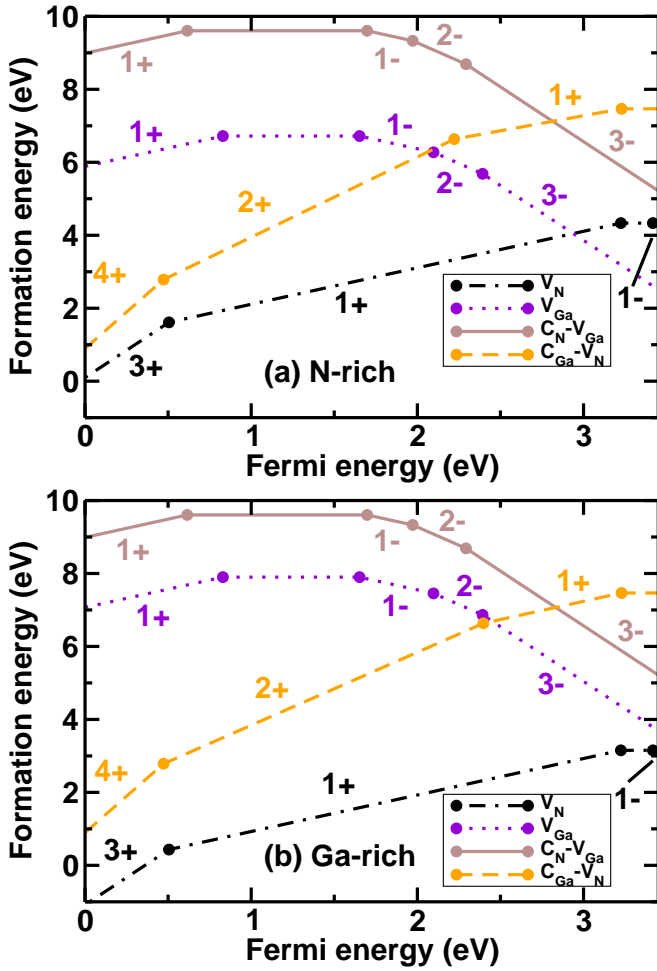


FIG. 8. Formation energies as a function of Fermi energy for $C_N - V_{Ga}$ (solid line in brown) and $C_{Ga} - V_N$ (dashed line in orange) in (a) N-rich conditions and (b) Ga-rich conditions. Formation energies for V_N (dashed-dotted line in black) and V_{Ga} (dotted line in violet) are also plotted for comparison.

complex considered here, up to mid-gap. On the other hand, in the N-rich limit, this complex is never favorable. Fig. 9 shows that binding energy for this complex is decreasing when the Fermi level is approaching the CBM and eventually becomes negative at around 3.38 eV.

In the 3+ charge state, this complex assumes an octahedral C-C configuration as indicated in Fig. 11(a). Both the 1+ and 0 (neutral) charge states, are found to be in the Type 2 C-C interstitial configuration, as shown in Fig. 11(c). The 1+ charge state of $C_I - C_N$ is also studied in Ref. 28. The reported values of 2.62 eV binding energy and 1.23 Å of C-C bond length are in good agreement with our results.

The C-C bond lengths and formation energies in each charge state are summarized in Table V together with previous LDA results¹⁴ for comparison.

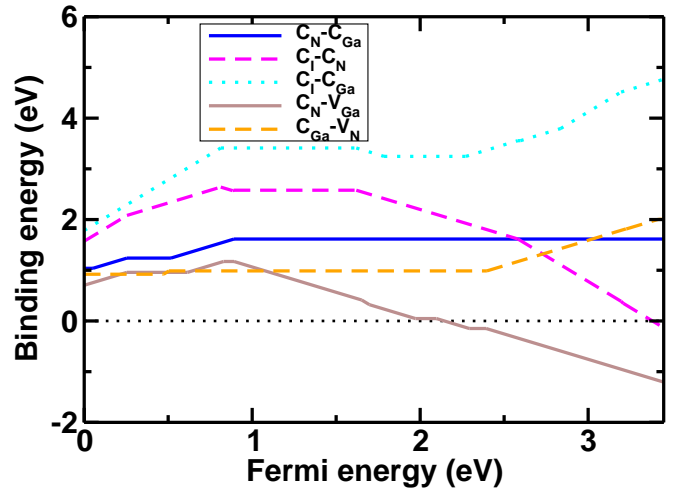


FIG. 9. Binding energies as a function of Fermi energy for $C_N - C_{Ga}$ (solid line in blue), $C_I - C_N$ (dashed line in magenta), $C_I - C_{Ga}$ (dotted line in cyan), $C_N - V_{Ga}$ (solid line in brown) and $C_{Ga} - V_N$ (dashed line in orange).

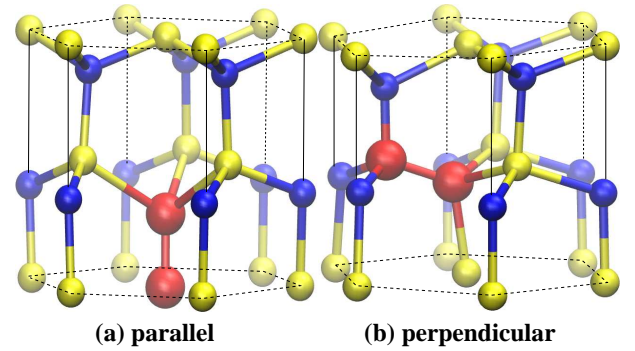


FIG. 10. Ball and stick representations of $C_N - C_{Ga}$ complex. (a) C_N and C_{Ga} are located parallel to the c -axis. (b) C_N and C_{Ga} are located perpendicular to the c -axis.

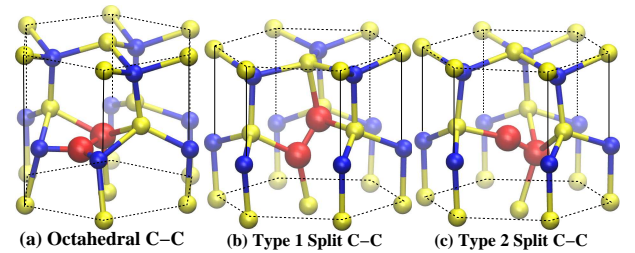


FIG. 11. Ball and stick representations of $C_I - C_N$ complex. (a) Octahedral C-C configuration: One of the C atoms is located at the octahedral interstitial position and the other is C_N . (b) Type 1 split C-C configuration: N atom of C-N dimer in Type 1 (and Type 2) split interstitial of C_I is replaced by C. (c) Type 2 split C-C configuration: N atom of C-N dimer in Type 3 (and Type 4) split interstitial of C_I is replaced by C.

TABLE V. Comparison of the calculated structural and electronic properties of $C_I - C_N$ in the different charge states q between the previous result in LDA¹⁴ and this work in HSE. The preferred forms with lowest energies in each charge state, the C-C bond lengths (l_{C-C} in Å) and the formation energies (E_f in eV) in Ga-rich conditions are presented.

q	form	LDA ^a		HSE (this work)		
		l_{C-C}	E_f	form	l_{C-C}	E_f
3+	octahedral	1.41	$2.65 + 3E_F$	octahedral	1.43	$1.34 + 3E_F$
1+	split 1	1.24	$3.88 + E_F$	split 2	1.29	$3.11 + E_F$
0	-	-	-	split 2	1.23	6.32

^a Ref. 14.

4. $C_I - C_{Ga}$

Two different configurations are obtained after relaxing the structure of the $C_I - C_{Ga}$ complex. One configuration is associated to the 3+, 2+ and 1+ charge states, in which a C-C dimer replaces a Ga atom and both high- and low-positioned C atoms have two bonds with surrounding N atoms. This is a Type 3 split C-C configuration as shown in Fig. 12(a). The other configuration is obtained for the neutral and 1- charge states, in which the high-positioned C atom has three bonds and the low-positioned one has one bond with surrounding N atoms. This is a Type 4 split C-C configuration as depicted in Fig. 12(b). In Ref. 14, another configuration, presented in Fig. 12(c), was reported to be a stable structure, but in our calculation we find that it never becomes energetically favorable. Formation energy values obtained for the $C_I - C_{Ga}$ complex are plotted (dotted lines) in Fig. 7. The 3+, 2+, 1+, 0 (neutral) and 1- charge states are available for values of the Fermi energy within the band gap. Moreover, the 3+ charge state is favorable for energies up to 1.79 eV. In N-rich limit, the $C_I - C_{Ga}$ complex with 3+ charge state is the most favorable among the C-related complexes considered here. In Ga-rich limit, the 3+ charge state of this complex together with same charge state of $C_I - C_N$ are the most favorable near the valence band maximum. Furthermore, the $C_I - C_{Ga}$ 2+ charge state is available up to 2.27 eV, followed by the 1+ charge state that is favorable up to 2.60 eV. Above 2.60 eV, the 0 (neutral) charge state is the most favorable. Finally, the -1 charge state becomes the most favorable above 2.84 eV. Thus, this complex shows amphoteric behavior, similar to C_I . However, charge states other than the 3+ have higher formation energies than $C_N - C_{Ga}$ and/or $C_I - C_N$. Fig. 9 shows that this complex forms with binding energy around 2 eV which subsequently increases above this value for Fermi energies in the upper half of the band gap. Note that, despite its high binding energy, the formation of this complex may be hindered, in particular, in p -type GaN (lower half of the band gap), because both C_{Ga} and C_I are positively charged and are expected to repel each other. The C-C bond lengths and formation energies in each charge state are summarized in Table VI together with previous LDA results¹⁴ for comparison.

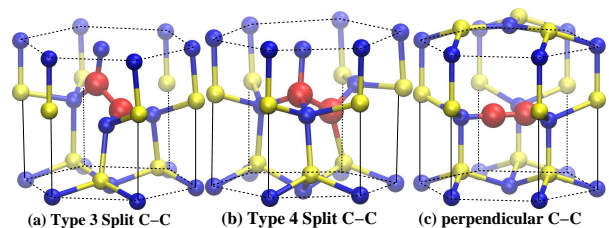


FIG. 12. Ball and stick representations of $C_I - C_{Ga}$ complex. a tilted C-C dimer replaces a Ga atom. (a) Type 3 split C-C configuration: both higher and lower C atoms have two bonds with surrounding N atoms. (b) Type 4 split C-C configuration: higher C atom has three bonds and the lower C atom has one bond with surrounding N atoms. (c) The C-C dimer is perpendicular to the c -axis and the N atom above the dimer takes a planar configuration with the surrounding three Ga atoms.

5. $C_N - V_{Ga}$

Both gallium and nitrogen vacancies were historically well investigated as parts of native defects in GaN. Earlier theoretical studies are based on the standard DFT (LDA and GGA)⁵²⁻⁵⁴. Recently hybrid functionals are used increasingly⁵⁵⁻⁵⁷. Here we studied the complexes made of substitutional carbon and vacancy. In this subsection the results for $C_N - V_{Ga}$ are given. Then the results of $C_{Ga} - V_N$ will be presented in the following subsection.

Two different configurations are found to be favorable for this complex. In one configuration, C_N and V_{Ga} are located parallel to the c -axis, as shown in Fig. 13(a). In the other configuration, C_N and V_{Ga} are located perpendicular to the c -axis, as depicted in Fig. 13(b). Both configurations have very similar formation energies, with less than 0.05 eV difference, but the parallel configuration possesses slightly lower formation energies.

Formation energy values obtained for the $C_N - V_{Ga}$ complex are plotted in Fig. 7 with brown solid line. The 1+, 0 (neutral) and 1-, 2- and 3- charge states are present in the band gap. As opposed to previous LDA calculations¹⁴ in which this complex was found to behave only as a deep acceptor, the present result indicates that $C_N - V_{Ga}$ shows amphoteric behavior. The (+/0) donor level appears at 0.61 eV above the valence band edge, while the (0/-), (-/2-) and (2-/3-) acceptor

TABLE VI. Comparison of structural and electronic properties of $C_1 - C_{Ga}$ in the different charge states q between the previous result in LDA¹⁴ and this work in HSE. The preferred forms with lowest energies in each charge state, the C-C bond lengths (l_{C-C} in Å) and the formation energies (E_f in eV) in Ga-rich conditions are presented.

q	form	LDA ^a		HSE (this work)		
		l_{C-C}	E_f	form	l_{C-C}	E_f
3+	split 3	1.43	$1.94 + 3E_F$	split 3	1.45	$1.41 + 3E_F$
2+	split 3	–	$3.94 + 2E_F$	split 3	1.43	$3.19 + 2E_F$
1+	split 3	–	$6.22 + E_F$	split 3	1.41	$5.47 + E_F$
0	\perp	1.43	8.48	split 4	1.51	8.06
1–	\perp	–	$10.13 - E_F$	split 4	1.35	$10.90 - E_F$

^a Ref. 14.

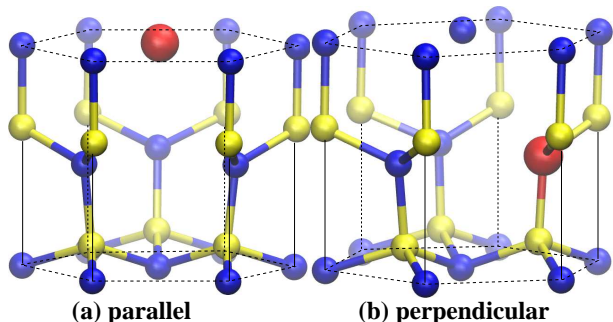


FIG. 13. Ball and stick representations of $C_N - V_{Ga}$ complex. V_{Ga} is located at the center of hexagonal prism. (a) C_N and V_{Ga} are located parallel to the c -axis. (b) C_N and V_{Ga} are located perpendicular to the c -axis.

levels are at 1.70, 1.97 and 2.29 eV, respectively. Examining the binding energy of this complex, from Fig. 9 it can be seen that at 2.14 eV above the valence band edge the binding energy becomes negative and the complex can no longer be stable. In addition, in n -type GaN (upper half of the band gap), both C_N and V_{Ga} are negatively charged and are expected to repel each other. This may impede the formation of this complex in n -type GaN. The C-C bond lengths and formation energies in each charge state are summarized in Table VII together with previous LDA results¹⁴ for comparison.

6. $C_{Ga} - V_N$

Similarly to the previous case, the $C_{Ga} - V_N$ complex is also found to assume parallel and perpendicular configurations. They are presented in Figs. 14(a) and (b), respectively. In the parallel configuration, C_{Ga} and V_N are located parallel to the c -axis and in the perpendicular configuration, C_{Ga} and V_N are located perpendicular to the c -axis. Once again, both configurations have very similar formation energies. In the 4+ and 2+ charge states, the perpendicular configuration is slightly more stable than the parallel configuration, whereas in the 1+ and the 0 (neutral) charge states, the parallel configuration is slightly more stable than the perpendicular con-

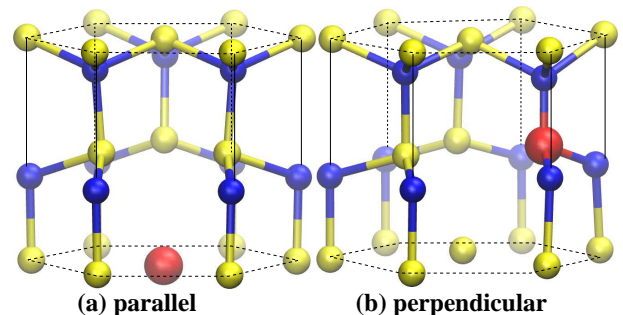


FIG. 14. Ball and stick representations of $C_{Ga} - V_N$ complex. V_N is located at the center of hexagonal prism. (a) C_{Ga} and V_N are located parallel to the c -axis. (b) C_{Ga} and V_N are located perpendicular to the c -axis.

figuration.

Formation energy values obtained for $C_{Ga} - V_N$ complex are plotted in Fig. 7 with orange dashed line. The 4+, 2+, 1+ and 0 (neutral) charge states are present in the band gap. Therefore, $C_{Ga} - V_N$ complex behaves as a potential donor. The 4+ charge state is favorable up to 0.47 eV above the valence band edge. Subsequently the 2+ charge state up to 2.40 eV and the 1+ charge state up to 3.23 eV become favorable. Finally the 0 (neutral) charge state becomes the most favorable above 3.23 eV. The binding energy of this complex, shown in Fig. 9, is at least 0.92 eV (close to the VBM) and eventually increases to 2 eV (close to the CBM). Consequently, the $C_{Ga} - V_N$ complex is stable for all values of Fermi energy within the band gap. However, in p -type GaN, both C_{Ga} and V_N are positively charged and are expected to repel each other. Thus, in p -type GaN the formation of this complex may be impeded. The C-V distances and formation energies in each charge state are summarized in Table VIII.

IV. DISCUSSION

This section presents a comparison between the experimental data available in the literature and the calculated results that have been outlined in the previous section. In general we expect that, based on Eq. (4), de-

TABLE VII. Comparison of structural and electronic properties of $C_N - V_{Ga}$ in the different charge states q between the previous result in LDA¹⁴ and this work in HSE. The preferred forms with lowest energies in each charge state, the C- V_{Ga} distances (d_{C-V} in Å), where the V_{Ga} position is taken to be the center of mass for the six surrounding Ga atoms, and the formation energies (E_f in eV) are presented.

q	LDA ^a			HSE (this work)		
	form	d_{C-V}	E_f	form	d_{C-V}	E_f
1+	–	–	–		2.21	$8.99 + E_F$
0	/⊥	–	9.85		2.00	9.60
1–	⊥	–	$10.11 - E_F$		2.05	$11.30 - E_F$
2–	⊥	–	$10.73 - 2E_F$		2.08	$13.27 - 2E_F$
3–	⊥	–	$12.09 - 3E_F$		2.12	$15.57 - 3E_F$
4–		–	$14.17 - 4E_F$		2.01	$20.06 - 4E_F$

^a Ref. 14.

TABLE VIII. The preferred forms with lowest energies in each charge state, the C- V_N distances (d_{C-V} in Å), where the V_N position is taken to be the center of mass for the six surrounding N atoms, and the formation energies (E_f in eV) are presented.

q	HSE (this work)		
	form	d_{C-V}	E_f
4+	⊥	2.52	$0.90 + 4E_F$
2+	⊥	2.54	$1.84 + 2E_F$
1+		2.30	$4.24 + E_F$
0		2.07	7.47

fects and complexes with lower formation energies may be present in higher concentrations and be the dominant carbon forms. However, this does not exclude the existence of other forms of the impurities. For example, in the case of n -type material, in which the Fermi energy is located in the upper half of the band gap, C_N with -1 charge state is expected to have the lowest formation energy among all kinds of C-related defects considered here. Therefore, C_N is expected to be the dominant form of carbon inclusion. However, recent experimental results suggest that, along with C_N , other form of carbon are present in bulk GaN⁵⁸. Among the carbon-carbon and carbon-vacancy complexes studied in this manuscript, $C_N - C_{Ga}$ and $C_N - V_{Ga}$ have the lowest formation energies in n -type GaN. Therefore they are also possible candidates for the carbon related defects commonly observed in GaN, although their formation energies are still much higher than that of C_N . However, we avoid for the moment making any statement about the possible dominant type of carbon inclusions and simply compare the calculated trap level with the measured one and try to identify which of the carbon-related defects or complexes may be responsible for it. Detailed analysis considering the impurity concentration will be done in the subsequent paper³⁰, after examining all types of carbon related complexes.

As already pointed out in Section I, a number of experiments have been performed to try to identify carbon-related traps in GaN. Table IX summarizes the experimental data available in the literature.

Activation energies are experimentally determined using two main techniques: DLTS and DLOS that use

thermal ionization and optical ionization of traps respectively. DLTS provides information on the thermal activation energy (E_{TH}), whereas DLOS on the optical activation energy (E_{OPT}). The difference between E_{TH} and E_{OPT} is schematically depicted in Fig. 15, where only the electron capture process is described⁵⁹. Specifically, d_{FC1} and d_{FC2} are the Franck-Condon shifts, which are the energies transferred to the lattice due to the relaxation process between the two equilibrium configurations in the respective charge states. Furthermore, from Fig. 15 we find that $E_{OPT} = E_{TH} + d_{FC2}$.

Armstrong²⁰ and coworkers investigated five trap levels that were determined to be C-related. Among these, a trap observed at $E_c - 3.0$ eV by DLOS and another trap at $E_v + 0.9$ eV by DLTS were considered to have the same origin. Additionally, trap levels at $E_c - 1.35$ eV, $E_c - 3.28$ eV and $E_c - 0.11$ eV were assigned to C_I ($0/2-$), C_N ($0/-$) and C_{Ga} ($+/0$), respectively. The origins of the other two levels, $E_c - 3.0/E_v + 0.9$ eV and $E_c - 1.94/2.05$ eV, were not specified. The results obtained by Shah *et al.*²³ point to three trap levels. One of them located at $E_c - 0.13$ eV was assigned to C_{Ga} ($+/0$). The trap levels at $E_c - 2.69$ eV and $E_c - 3.20$ eV were assumed to be related to C_N . The latter was assigned to C_N ($0/-$), whereas the former to a C_N related complex or gallium vacancies. Using room temperature photocurrent measurement, Polyakov *et al.* found three optical thresholds corresponding to $E_c - 1.3/1.4$ eV, $E_c - 2.7/2.8$ eV and $E_c - 3$ eV. The first one was attributed to C_I ($0/2-$) level, while the other two levels were not assigned. The assignments of the trap levels to specific carbon related defects performed by three experimental groups consid-

TABLE IX. Experimentally observed C-related trap levels. Activation energies obtained by thermal methods such as DLTS and by optical methods such DLOS are denoted by E_{TH} and E_{OPT} , respectively (in eV).

Armstrong <i>et al.</i> ^a	Shah <i>et al.</i> ^b	Polyakov <i>et al.</i> ^c	Honda <i>et al.</i> ^d
$E_c - E_{\text{OPT}}$	$E_c - E_{\text{TH}}/E_v + E_{\text{TH}}$	$E_c - E_{\text{OPT}}$	$E_c - E_{\text{TH}}/E_v + E_{\text{TH}}$
$E_c - 1.35$	$E_c - 0.11$	$E_c - 0.13$	$E_c - 0.40$
$E_c - 3.0$	$E_v + 0.9$	$E_c - 2.69$	$E_v + 0.86$
$E_c - 3.28$		$E_c - 3.20$	
$E_c - 1.94/2.05$		$E_c - 3$	

^aRef. 20. ^bRef. 23. ^cRef. 24. ^dRef. 22.

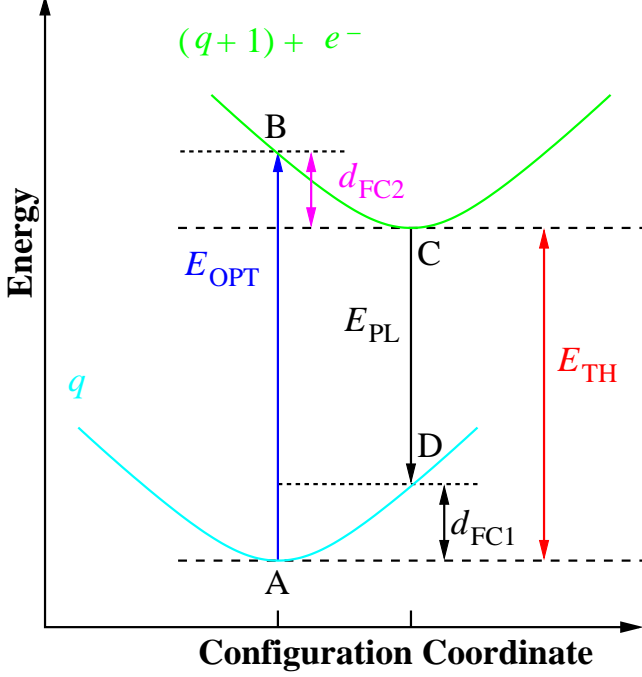


FIG. 15. Schematic configuration coordinate diagram of the electron capture process to show the relationship between thermal activation energy (E_{TH}) and optical activation energy (E_{OPT}).

ered above were carried out on the basis of existing LDA results. Finally, Honda and coworkers²² using DLTS and MCTS observed three C-related trap levels. Unfortunately, energy levels for only two of them were reported. One at $E_c - 0.40$ eV and the other at $E_v + 0.86$ eV. Using HSE calculated energy²⁶, $E_v + 0.86$ eV was assigned to $C_N(0/-)$, while the origin of the trap at $E_c - 0.40$ eV was not specified.

The formation energy values presented in Sec. III A and Sec. III B were computed under the assumption of thermodynamic equilibrium. As a result, the transition between the levels of two charge states (q/q') is characterized using a quantity called thermal ionization energies. With reference to Fig. 15, we define E_{TH} as the energy difference between configurations C and A, $E_c - E_A$ that is defined as $E_f^{q+1} + E_g - E_f^q$, where E_g is the energy, corresponding to the band gap, necessary to add an elec-

tron to the conduction band. Furthermore, E_{TH} can also be expressed as $E_{\text{TH}} = E_g - \varepsilon(q/q + 1)$, using Eq. (3). Similarly, from Fig. 15 E_{OPT} is defined as the energy difference between the configurations B and A or $E_B - E_A$. Specifically, E_B is calculated starting from the formation energy of the state having the geometry of A with a charge state $q + 1$ and adding E_g to account for the energy necessary to promote an electron to the conduction band.

Using the previously derived relationships, both thermal and optical activation energies obtained by our calculations are summarized in Tables X for single impurity carbon, and XI for carbon complexes. We point out that in these tables we also report transition levels involving thermodynamically unstable charge states: $(4+/3+)$ and $(3+/2+)$ of C_I , $(3+/2+)$ and $(2+/+)$ of $C_I - C_N$, $(4+/3+)$ and $(3+/2+)$ of $C_{Ga} - V_N$, which are experimentally accessible using dynamical techniques such as DLTS and DLOS. Furthermore, values that are reported in bold and enclosed in a box are the proposed assignment emerging from our numerical analysis.

We consider first the trap level located at $E_c - 3.0/E_v + 0.9$ eV obtained by Armstrong *et al.* and that was also observed by Polyakov *et al.* as well as by Honda *et al.*. While Armstrong *et al.* and Polyakov *et al.* did not give a clear assignment to this trap level, Honda *et al.*²² assigned it to $C_N(0/-)$ by comparing the experimental value to the calculated result obtained using HSE by Lyons *et al.*²⁶. Indeed our calculated results support this assignment. In our case, the $C_N(0/-)$ level is located at 0.89 eV above valence band maximum with 2.91 eV optical activation energy (E_{OPT}) as shown in Table X. Furthermore, the thermal activation energy of this trap is calculated to be $E_{\text{TH}} = 2.56$ eV. This value is in good agreement with the value of 2.60 eV reported in Ref. 28, where its assignment was done for the onset near 2.5 eV by the photoluminescence excitation data⁶⁰. In addition to the $C_N(0/-)$ level, $C_I(4+/2+)$ level is located at 0.81 eV above the VBM, which corresponds to the 2.64 eV thermal activation energy (Table X). Related optical activation energy, $C_I(4+/3+)$ is calculated as 3.11 eV, which is close to the experimental value $E_c - 3.0$ eV. Similarly, the $(3+/+)$ level of $C_I - C_N$, is positioned at 0.88 eV above the VBM with $E_{\text{TH}} = 2.57$ eV (Table XI). Consequently we argue that the trap level at $E_c - 2.69$ eV, originally measured by Shah *et al.*²³ and that was considered to be related to

TABLE X. Thermodynamic transition levels [$\varepsilon(q/q')$], thermal activation energies (E_{TH}) and optical activation energies (E_{OPT}) obtained from our calculated results for single impurity of C. The levels which do not appear within the band gap are denoted as horizontal bar. The energy levels close to the experimental ones are denoted in bold.

Form	(q/q')	$\varepsilon(q/q')$	E_{TH}	E_{OPT}
C_{Ga}	(+/0)	–	–	–
	(0/–)	–	–	–
C_{N}	(+/0)	0.25	3.20	–
	(0/–)	0.89	2.56	2.91
C_{I}	(4+/2+)	0.81	2.64	–
	(4+/3+)	2.63	0.82	3.11
	(3+/2+)	–	–	–
	(2+/+)	1.62	1.83	2.87
	(+/0)	2.58	0.87	1.58
	(0/–)	3.20	0.25	0.82

TABLE XI. Thermodynamic transition levels [$\varepsilon(q/q')$], thermal activation energies (E_{TH}) and optical activation energies (E_{OPT}) obtained from our calculated results for C complexes. The levels which do not appear within the band gap are denoted as horizontal bar. The energy levels close to the experimental ones are denoted in bold.

Form	(q/q')	$\varepsilon(q/q')$	E_{TH}	E_{OPT}
$C_{\text{N}} - C_{\text{Ga}}$	(2+/+)	0.05	3.40	–
	(+/0)	0.52	2.93	–
$C_{\text{I}} - C_{\text{N}}$	(3+/+)	0.88	2.57	–
	(3+/2+)	2.28	1.17	–
	(2+/+)	–	–	–
	(+/0)	3.21	0.24	1.03
$C_{\text{I}} - C_{\text{Ga}}$	(3+/2+)	1.79	1.66	2.79
	(2+/+)	2.27	1.18	1.96
	(+/0)	2.60	0.85	1.47
	(0/–)	2.84	0.61	1.31
$C_{\text{N}} - V_{\text{Ga}}$	(+/0)	0.61	2.84	3.21
	(0/–)	1.70	1.75	2.08
	(–/2–)	1.97	1.48	1.49
	(2–/3–)	2.29	1.16	1.27
$C_{\text{Ga}} - V_{\text{N}}$	(4+/2+)	0.47	2.98	–
	(4+/3+)	0.55	2.90	–
	(3+/2+)	0.40	3.05	–
	(2+/+)	2.40	1.05	2.13
	(+/0)	3.23	0.22	1.06

C_{N} complex or gallium vacancy, is in reality due to C_{N} (0/–) with possible contributions from C_{I} and $C_{\text{I}} - C_{\text{N}}$.

We turn our attention to the trap levels originally assigned to C_{N} (0/–), specifically the one located at $E_c - 3.28$ eV measured by Armstrong *et al.* and $E_c - 3.20$ eV level by Shah *et al.*. Since Shah *et al.* measured this energy with MCTS we assume that this is a thermal activation energy. From Tables X and XI we can observe that the energies corresponding to (+/0) of C_{N} gives the value of 3.20 eV. On the other hand, we notice that the trap level observed by Armstrong *et al.* with DLOS should be treated as an optical activation energy. In this case we observe that the (+/0) of $C_{\text{N}} - V_{\text{Ga}}$ (3.21 eV) is calculated as an optical trap level, which has the energy very close to experimental one (3.28 eV).

The next one is the trap level at $E_c - 1.35$ eV observed by Armstrong *et al.* and Polyakov *et al.* that was assigned to C_{I} (0/2–) based on a 1.13 eV thermal activation energy computed by LDA¹⁴. First we point out that, based on our HSE calculation, the (0/2–) state is energetically unfavorable while the (0/–), that was found to be unfavorable with LDA, is now possible. For this (0/–) state we compute an optical activation energy of 0.82 eV that corresponds to a thermal activation energy of 0.25 eV. Consequently, C_{I} (0/–) cannot be the origin of the level $E_c - 1.35$ eV observed by Armstrong *et al.* and Polyakov *et al.* Additionally, we notice that the calculated (+/0) C_{I} level from HSE results in a optical activation energy of 1.58 eV, corresponding to a thermal activation energy of 0.87 eV. Therefore based on our re-

sults, the origin of $E_c - 1.35$ eV level is not likely to be related to any of the C_I states. Finally, based on HSE the $(0/-)$ and $(+/0)$ states of the $C_I - C_{Ga}$ complex have a 1.31 eV and 1.47 eV optical activation energies, respectively. As a result, $C_I - C_{Ga}$ is likely to be the origin of the experimentally observed $E_c - 1.35$ eV level. Note that the $(-/2-)$ and $(2-/3-)$ states of the $C_N - V_{Ga}$ complex have $E_{OPT} = 1.27$ eV and 1.49 eV, respectively, but this complex is unstable in this energy region with negative or barely positive binding energies (Fig. 9).

Honda *et al.* observed, using DLTS, a $E_c - 0.40$ eV level and concluded that it was C-related, but did not mention its origin. Based on our calculations the $(0/-)$ level of C_I has a 0.25 eV thermal activation energy. Furthermore, the theoretical values of the activation energy for the $(+/0)$ level of $C_{Ga} - V_N$ is 0.22 eV. Therefore, it is likely that the origin of the $E_c - 0.40$ eV level is the $(0/-)$ state of C_I and/or the $(+/0)$ state of $C_{Ga} - V_N$. The $(+/0)$ level of $C_I - C_N$ has $E_{TH} = 0.24$ eV. However, at this energy range this complex is unlikely to form due to the barely positive binding energy.

The $E_c - 1.94/2.05$ eV level observed with DLOS by Armstrong *et al.* was assumed to be C-related but its physical form remained unknown. From our calculated results two levels have similar optical activation energies. One is $(2+/+)$ level of $C_I - C_{Ga}$ with 1.96 eV and the other is $(2+/+)$ level of $C_{Ga} - V_N$ with 2.13 eV. These two states are the likely candidates to explain the physical origin of the $E_c - 1.94/2.05$ eV trap level. The $(0/-)$ level of weakly bounded $C_N - V_{Ga}$ with $E_{OPT} = 2.08$ eV is unlikely to contribute.

Polyakov *et al.* observed a optical threshold at 2.7–2.8 eV by photocurrent spectra measurement. The origin of this trap level is likely to be the $(2+/+)$ level of C_I and/or the $(3+/2+)$ level of $C_I - C_{Ga}$, whose optical activation energies are computed to be 2.87 eV and 2.79 eV, respectively.

The last two energy levels we consider are the one located at $E_c - 0.11$ eV measured by Armstrong *et al.* and at $E_c - 0.13$ eV measured by Shah *et al.*. These two levels were assigned to C_{Ga} based on LDA results¹⁴, for which the $(+/0)$ transition level was computed to be about 0.2 eV below CBM. However, our HSE calculation shows that such $(+/0)$ level of C_{Ga} does not appear within the band gap, but it is in the conduction band approximately 0.5 eV above the CBM. Recent HSE calculation by Lyons *et al.*²⁸ does not show such level within the band gap either. From our results we evince that the $(+/0)$ level of $C_I - C_N$ complex has a 0.24 eV thermal activation energy. Unfortunately this complex is unlikely to form when the Fermi energy is around this value because its binding energy is barely positive as we can see from Fig. 9. Based on our calculations, the most likely candidate is the $(+/0)$ state of $C_{Ga} - V_N$ located at 0.22 eV below the CBM and/or the $(0/-)$ state of C_I at 0.25 eV below the CBM. Therefore, it is probable that these levels have the same origin of the $E_c - 0.40$ eV level observed by Honda *et al.*

TABLE XII. Vibrational frequencies for C_I , $C_I - C_{Ga}$ and $C_I - C_N$ (in cm^{-1}). The breathing modes are given in the 4+ and 3+ charge states of C_I and the stretching modes are given in the other charge states of C_I and all the charge states of $C_I - C_{Ga}$ and $C_I - C_N$.

Form	q	vibrational frequency
C_I	4+	1004
	2+	2213
	1+	1839
	0	1546
	1-	1279
$C_I - C_{Ga}$	3+	1455
	2+	1462
	1+	1459
	0	1090
	1-	1574
$C_I - C_N$	3+	1246
	1+	2049

Finally, we also calculated vibrational frequencies of relevant charge states in the cases of C_I , $C_I - C_{Ga}$ and $C_I - C_N$ complexes. Our calculations are based on the finite difference method also implemented in the VASP code, where small (both positive and negative by 0.015 Å) displacements are introduced. These local vibrational modes may provide alternative information for the experimental detection of these carbon related impurities. The frequencies for the breathing modes in the 4+ and 3+ charge states of C_I and for the stretching modes in the other charge states of C_I and all the charge states of $C_I - C_N$ and $C_I - C_{Ga}$ are summarized in Table XII.

V. CONCLUSION

We have performed first-principles calculations using HSE hybrid density functional in the framework of DFT to investigate the characteristics of various forms of carbon inclusions in GaN. We have considered single impurities, C_N , C_{Ga} and C_I , as well as their complexes $C_N - C_{Ga}$, $C_I - C_N$, $C_I - C_{Ga}$, $C_N - V_{Ga}$ and $C_{Ga} - V_N$. For all these configurations, different charge states have been considered and their geometries are fully optimized. Formation and binding energies of complexes have been computed and thermodynamic transition levels are obtained.

Among single impurities, C_N behaves mainly as a deep acceptor, C_{Ga} acts as a donor without inducing states in the band gap and C_I shows amphoteric behavior. Both in N-rich and Ga-rich conditions the 4+ charge state of C_I , which assumes an octahedral interstitial position, is favorable close to the VBM (p -type region). The 1- charge state of C_N is favorable close to the CBM (n -type region), and C_{Ga} is also favorable in p -type region but only in N-rich conditions.

Complexes made of combinations of single impurities, specifically $C_N - C_{Ga}$, $C_I - C_N$ and $C_I - C_{Ga}$, have also

been considered. $C_N - C_{Ga}$ is favorable in the upper half of the band gap (n -type) region, whereas $C_I - C_N$ and $C_I - C_{Ga}$ are favorable in the lower half of the band gap (p -type) region. Finally, Complexes with vacancies are also examined, in particular $C_N - V_{Ga}$ and $C_{Ga} - V_N$. The former is favorable with lower formation energy comparing to the latter close the CBM, but is unstable as a complex in the n -type region with negative value of binding energy. The latter is favorable in the p -type region comparing to the former.

From the calculated formation energies we have evaluated the thermodynamic transition levels. These are directly related to the thermal activation energies observed in experimental techniques such as DLTS. In addition, by calculating Franck-Condon shift, optical activation energies, which can be obtained by optical techniques such as DLOS, have been evaluated from the thermal activation energies. We compare our calculated values of activation energies with the energies of experimentally observed C-related trap levels.

Using the information on the transition levels we have assigned the C-related trap levels, whose physical form was unknown before. It should be noted that these assignments are performed based only on the positions of the trap levels and their concentrations are not taken into account. The trap level observed at $E_c - 3/E_v + 0.9$ eV is likely due to the $(0/-)$ level of C_N with possible contributions from C_I and $C_I - C_N$. Based on earlier investigations performed employing LDA, two different energy levels: $E_c - 3.2$ eV level by MCTS (thermal method) and $E_c - 3.28$ eV by DLOS (optical method), were attributed to the $(0/-)$ level of C_N . However, our HSE calculation shows that the origin of the $E_c - 3.2$ eV level is the $(+/0)$ level of C_N and of the level at $E_c - 3.28$ eV is the $(+/0)$ of $C_N - V_{Ga}$.

Based on LDA results, the trap level observed at $E_c - 1.35$ eV was unanimously attributed to the $(0/2-)$ state of C_I . However, the outcome of our HSE calculation suggests its origin is the $(0/-)$ and/or $(+/0)$ states of

the $C_I - C_{Ga}$ complex. The trap at $E_c - 1.94/2.05$ eV is likely due to two configurations. One is the $(2+/+)$ of $C_I - C_{Ga}$ and the other is the $(2+/+)$ of $C_{Ga} - V_N$. Looking at the trap level located at $E_c - 2.7/2.8$ eV we argue that its origin stems from the $(2+/+)$ state of the C_I and the $(3+/2+)$ state of the $C_I - C_{Ga}$.

Multiple contributors are likely to be responsible for the trap at $E_c - 0.4$ eV. Specifically we find that the $(0/-)$ of C_I and the $(+/0)$ of $C_{Ga} - V_N$ have energies that are close to the measured value. Finally, the trap at $E_c - 0.1$ eV was attributed to C_{Ga} based on LDA results. However, based on our HSE calculations, there are no gap states due to C_{Ga} . Therefore the origin of this trap level is still unclear, but the most likely candidate is the $(+/0)$ of $C_{Ga} - V_N$ and/or the $(0/-)$ of C_I . In this case these levels have same origin as $E_c - 0.40$ eV level.

Our calculated LVM results would provide additional information for the experimental detection of these carbon related impurities.

ACKNOWLEDGMENTS

The authors thank K. Jones and R. Tompkins of the Army Research Laboratory and T. Moustakas of Boston University for many discussions and their help in understanding the experimental techniques. The authors are grateful to A. F. Wright, S. Lee and N. Modine from Sandia National Laboratory and S. Sharifzadeh of Boston University for discussing the results of our work.

The authors gratefully acknowledge financial support from the U. S. Army Research Laboratory through the Collaborative Research Alliance (CRA) Grant No. W911NF-12-2-0023 for MultiScale multidisciplinary Modeling of Electronic materials (MSME). This work was performed using DoD HPCMP supercomputing resources and computational resources provided by the 2014 Army Research Office Grant No. W911NF-14-1-0432 DURIP Award made to E. Bellotti.

-
- ¹ D. Koleske, A. Wickenden, R. Henry, and M. Twigg, *Journal of Crystal Growth* **242**, 55 (2002).
 - ² A. Wickenden, D. Koleske, R. Henry, M. Twigg, and M. Fatemi, *Journal of Crystal Growth* **260**, 54 (2004).
 - ³ S. W. King, J. P. Barnak, M. D. Bremser, K. M. Tracy, C. Ronning, R. F. Davis, and R. J. Nemanich, *Journal of Applied Physics* **84**, 5248 (1998).
 - ⁴ F. Machuca, Z. Liu, Y. Sun, P. Pianetta, W. E. Spicer, and R. F. W. Pease, *Journal of Vacuum Science & Technology A* **20**, 1784 (2002).
 - ⁵ G. Koblmüller, R. M. Chu, A. Raman, U. K. Mishra, and J. S. Speck, *Journal of Applied Physics* **107**, 043527 (2010).
 - ⁶ J. B. Webb, H. Tang, S. Rolfe, and J. A. Bardwell, *Applied Physics Letters* **75**, 953 (1999).
 - ⁷ Y. C. Choi, M. Pophristic, B. Peres, H.-Y. Cha, M. G. Spencer, and L. F. Eastman, *Semiconductor Science and Technology* **22**, 517 (2007).
 - ⁸ P. B. Klein, J. A. Freitas, S. C. Binari, and A. E. Wickenden, *Applied Physics Letters* **75**, 4016 (1999).
 - ⁹ G. Meneghesso, F. Rossi, G. Salviati, M. J. Uren, E. Muoz, and E. Zanoni, *Applied Physics Letters* **96**, (2010).
 - ¹⁰ P. Bogusławski, E. L. Briggs, and J. Bernholc, *Applied Physics Letters* **69**, 233 (1996).
 - ¹¹ P. Bogusławski and J. Bernholc, *Phys. Rev. B* **56**, 9496 (1997).
 - ¹² J. Neugebauer and C. G. V. de Walle, in *Festkörperprobleme/Advances in Solid State Physics*, Vol. 35, edited by R. Helbig (Springer-Verlag Berlin Heidelberg, 1995) pp. 25–44.
 - ¹³ J. A. Chisholm and P. D. Bristowe, *Journal of Physics: Condensed Matter* **13**, 8875 (2001).
 - ¹⁴ A. F. Wright, *Journal of Applied Physics* **92**, 2575 (2002).
 - ¹⁵ In this case we have used the term shallow acceptor/donor rather loosely. Obviously from the practical standpoint an

- activation energy larger than several thermal energies will lead to a small fraction of ionized donors and acceptors. Nevertheless, we will use the qualifiers shallow and deep to distinguish between states that are closer or farther from the CBM/VBM.
- ¹⁶ C. H. Seager, A. F. Wright, J. Yu, and W. Götz, *Journal of Applied Physics* **92**, 6553 (2002).
 - ¹⁷ P. B. Klein, S. C. Binari, K. Ikossi, A. E. Wickenden, D. D. Koleske, and R. L. Henry, *Applied Physics Letters* **79**, 3527 (2001).
 - ¹⁸ A. Hierro, D. Kwon, S. A. Ringel, M. Hansen, J. S. Speck, U. K. Mishra, and S. P. DenBaars, *Applied Physics Letters* **76**, 3064 (2000).
 - ¹⁹ A. Armstrong, A. R. Arehart, B. Moran, S. P. DenBaars, U. K. Mishra, J. S. Speck, and S. A. Ringel, *Applied Physics Letters* **84**, 374 (2004).
 - ²⁰ A. Armstrong, A. R. Arehart, D. Green, U. K. Mishra, J. S. Speck, and S. A. Ringel, *Journal of Applied Physics* **98**, 053704 (2005).
 - ²¹ Z.-Q. Fang, B. Clafin, D. C. Look, D. S. Green, and R. Vetury, *Journal of Applied Physics* **108**, 063706 (2010).
 - ²² U. Honda, Y. Yamada, Y. Tokuda, and K. Shiojima, *Japanese Journal of Applied Physics* **51**, 04DF04 (2012).
 - ²³ P. Shah, R. Dedhia, R. Tompkins, E. Viveiros, and K. Jones, *Solid-State Electronics* **78**, 121 (2012).
 - ²⁴ A. Y. Polyakov, N. B. Smirnov, E. A. Kozhukhova, A. V. Osinsky, and S. J. Pearton, *Journal of Vacuum Science & Technology B* **31**, 051208 (2013).
 - ²⁵ A. Armstrong, C. Poblentz, D. S. Green, U. K. Mishra, J. S. Speck, and S. A. Ringel, *Applied Physics Letters* **88**, 082114 (2006).
 - ²⁶ J. L. Lyons, A. Janotti, and C. G. Van de Walle, *Applied Physics Letters* **97**, 152108 (2010).
 - ²⁷ D. O. Demchenko, I. C. Diallo, and M. A. Reshchikov, *Phys. Rev. Lett.* **110**, 087404 (2013).
 - ²⁸ J. L. Lyons, A. Janotti, and C. G. Van de Walle, *Phys. Rev. B* **89**, 035204 (2014).
 - ²⁹ A. Alkauskas, Q. Yan, and C. G. Van de Walle, *Phys. Rev. B* **90**, 075202 (2014).
 - ³⁰ M. Matsubara and E. Bellotti, "A first-principles study of carbon-related energy levels in gan: Part II - complexes formed by carbon and hydrogen, silicon or oxygen," submitted to *J. Appl. Phys.* (2017).
 - ³¹ P. E. Blöchl, *Phys. Rev. B* **50**, 17953 (1994).
 - ³² G. Kresse and J. Furthmüller, *Phys. Rev. B* **54**, 11169 (1996); G. Kresse and D. Joubert, *ibid.* **59**, 1758 (1999).
 - ³³ J. Heyd, G. E. Scuseria, and M. Ernzerhof, *The Journal of Chemical Physics* **118**, 8207 (2003); **124**, 219906 (2006).
 - ³⁴ J. P. Perdew, K. Burke, and M. Ernzerhof, *Phys. Rev. Lett.* **77**, 3865 (1996).
 - ³⁵ B. Monemar, *Phys. Rev. B* **10**, 676 (1974).
 - ³⁶ Y.-N. Xu and W. Y. Ching, *Phys. Rev. B* **48**, 4335 (1993).
 - ³⁷ M. R. Ranade, F. Tessier, A. Navrotsky, V. J. Leppert, S. H. Risbud, F. J. DiSalvo, and C. M. Balkas, *The Journal of Physical Chemistry B* **104**, 4060 (2000).
 - ³⁸ H. Hahn and R. Juza, *Zeitschrift für anorganische und allgemeine Chemie* **244**, 111 (1940).
 - ³⁹ A. S. Barker and M. Ilegems, *Phys. Rev. B* **7**, 743 (1973).
 - ⁴⁰ C. Freysoldt, J. Neugebauer, and C. G. Van de Walle, *Phys. Rev. Lett.* **102**, 016402 (2009); *physica status solidi (b)* **248**, 1067 (2011).
 - ⁴¹ C. Freysoldt, "sxdefectalign," <https://sxrepo.mpie.de/projects/sphinx-add-ons/files>.
 - ⁴² G. Makov and M. C. Payne, *Phys. Rev. B* **51**, 4014 (1995).
 - ⁴³ S. Lany and A. Zunger, *Phys. Rev. B* **78**, 235104 (2008).
 - ⁴⁴ S. Lany and A. Zunger, *Modelling and Simulation in Materials Science and Engineering* **17**, 084002 (2009).
 - ⁴⁵ S. E. Taylor and F. Bruneval, *Phys. Rev. B* **84**, 075155 (2011).
 - ⁴⁶ H.-P. Komsa, T. T. Rantala, and A. Pasquarello, *Phys. Rev. B* **86**, 045112 (2012).
 - ⁴⁷ S. Lany and A. Zunger, *Phys. Rev. B* **81**, 205209 (2010).
 - ⁴⁸ Here the 4+ charge state was defined by removing four electrons from the whole system, not from the C atom. In fact, electron deficiency is localized around the C-N₃ (C and surrounding three N atoms) structure.
 - ⁴⁹ A. Alkauskas, P. Broqvist, and A. Pasquarello, *Phys. Rev. Lett.* **101**, 046405 (2008).
 - ⁵⁰ A. Alkauskas and A. Pasquarello, *Phys. Rev. B* **84**, 125206 (2011).
 - ⁵¹ G. Miceli and A. Pasquarello, *Microelectronic Engineering* **147**, 51 (2015), *insulating Films on Semiconductors 2015*.
 - ⁵² J. Neugebauer and C. G. Van de Walle, *Phys. Rev. B* **50**, 8067 (1994).
 - ⁵³ T. Mattila and R. M. Nieminen, *Phys. Rev. B* **55**, 9571 (1997).
 - ⁵⁴ M. G. Ganchenkova and R. M. Nieminen, *Phys. Rev. Lett.* **96**, 196402 (2006).
 - ⁵⁵ Q. Yan, A. Janotti, M. Scheffler, and C. G. Van de Walle, *Applied Physics Letters* **100**, 142110 (2012).
 - ⁵⁶ R. Gillen and J. Robertson, *Journal of Physics: Condensed Matter* **25**, 405501 (2013).
 - ⁵⁷ J. L. Lyons, A. Alkauskas, A. Janotti, and C. G. Van de Walle, *physica status solidi (b)* **252**, 900 (2015).
 - ⁵⁸ R. P. Tompkins, T. A. Walsh, M. A. Derenge, K. W. Kirchner, S. Zhou, C. B. Nguyen, K. A. Jones, P. Suvarna, M. Tungare, N. Tripathi, and F. S. Shahedipour-Sandvik, *Journal of Materials Research* **26**, 2895 (2011).
 - ⁵⁹ The hole capture process is not explicitly considered here because none of the experimental optical activation energies cited in this paper are obtained by the hole capture process.
 - ⁶⁰ T. Ogino and M. Aoki, *Japanese Journal of Applied Physics* **19**, 2395 (1980).